ISSN 1392-1207. MECHANIKA. Vol. 29, No. 6, 2023: 486–493

Analysis of Taxiing Performance of Single Strut Landing Gear Based on ISD

Yu WANG*, Changming ZHANG, Peng WANG***, Xuan CAO****, Zhan GE*****
**School of Mechanical Engineering, Shaanxi University of Technology, Hanzhong 723000, China, E-mail: 2248412718@qq.com*
***School of Mechanical Engineering, Shaanxi University of Technology, Hanzhong 723000, China; Engineering Research Center of Manufacturing and Testing for Landing Gear and Aircraft Structural Parts, Universities of Shaanxi Province, Hanzhong 723000, China, E-mail: zhangchangmingsx@126.com (Corresponding Author)*
****School of Mechanical Engineering, Shaanxi University of Technology, Hanzhong 723000, China*
*****School of Mechanical Engineering, Shaanxi University of Technology, Hanzhong 723000, China*
******School of Mechanical Engineering, Shaanxi University of Technology, Hanzhong 723000, China*

https://doi.org/10.5755/j02.mech.33571

1. Introduction

As one of the essential components of the aircraft landing gear, the buffer plays the role of bearing, shock absorption, and energy dissipation in the process of aircraft parking, take-off and landing, respectively. In order to improve the buffering performance of the landing gear buffer, its structural form has been continuously improved, and solid spring buffer, fluid spring buffer, and oleo-pneumatic buffer have appeared successively [1, 2]. The strongest power absorption capacity and maximum buffering effectiveness are found in the oleo-pneumatic buffer, which is why it is frequently utilized in landing gear [3].

Although the buffer's structure has continuously improved, its shock-absorption technique has remained the same. It still stores energy in a spring (solid, liquid, or gas) and dissipates it by using the damping qualities of oil flowing through the throttle hole. Based on the second type of electromechanical similarity theory, Professor Smith of the University of Cambridge proposed a mechanical element called inerter [4]. Later, the inerter was applied to automotive suspensions [5], train suspension systems [6], and building vibration isolations [7]. It demonstrated good performance in vibration reduction and isolation, which gave researchers a fresh perspective on the landing gear buffer's novel shock absorption mechanism. Dong [8] observed and analyzed the shimmy change of landing gear before and after the introduction of the inerter, and finally proved that the inerter has application value in restraining shimmy. Based on the shimmy model of the linear landing gear with inerter, Liu [9] considered the influence of nonlinear factors on shimmy. Li [10, 11] proposed a passive anti-shimmy device with an inerter, and found that it has a better anti-shimmy effect than the traditional passive anti-shimmy device. Under the condition that the maximum strut load and the maximum stroke of ISDLG (inerter-spring-damper landing gear) are not larger than that of SDLG (spring-damper landing gear), Li [12] took the highest strut efficiency as the optimization objective function to analyze the optimal layout of ISDLG. The above researches show that it is feasible to introduce the inerter into the landing gear.

The aircraft is subjected to random vibration caused by the uneven road surface during taxiing on the airport runway, which will cause fatigue damage and local damage to the elements on the one hand; On the other hand, it will affect the comfort of the personnel inside the aircraft. Therefore, the in-depth study of the aircraft during the taxiing stage is an indispensable part of ensuring the safe flight of the aircraft. Xu [13] and Qian [14] revealed the variation laws of the maximum overload at the center of gravity, the maximum vertical load on the tire, the maximum compression of the buffer, and the dynamic load coefficient of the aircraft taxiing with the taxiing speed and the road roughness through the multi-conditions taxiing simulation of the established aircraft model, respectively. Zhang [15] studied the taxiing performance of ISDLG under different static equilibrium positions, but he ignored the equivalent damping of the tires and did not optimize the parameters of elements in detail.

The above analysis shows the dearth of domestic and international research on ISDLG taxiing. As a result, this paper firstly establishes the taxiing dynamic models of a single strut SDLG and ISDLG based on the two-mass system. Secondly, the structural parameters of the ISDLG are optimized using a multi-objective genetic optimization algorithm. Finally, in order to study the influence of ISD on aircraft taxiing performance and to analyze the influence laws of different speeds and road grades on taxiing performance, MATLAB/Simulink is used to simulate the two models.

2. Taxiing dynamic model of single strut landing gear

Like spring and damper, the inerter is a mechanical device with two endpoints. In particular, the forces acting on the two endpoints are equal in magnitude, opposite in direction, and proportional to the relative acceleration between the two endpoints [16], as shown in Fig.1.

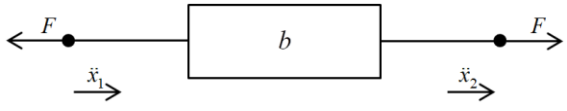

Fig. 1 The model of inerter

It can be expressed as:

$$F = b(\ddot{x}_1 - \ddot{x}_2), \tag{1}$$

where: b is the inertance in kg.

This paper mainly studies the change in aircraft taxiing performance before and after the introduction of inerter, so the influence of some nonlinear factors will be ignored during modeling, and the following assumptions are made [15]:

1. The vibration characteristics of the inerter, spring, damper, and tire are assumed to be linear;

2. All aircraft parts except tires are assumed to be rigid bodies;

3. Only vertical forces are considered, and the forces act in the same vertical plane;

4. The friction force and structural limiting force of the buffer are ignored.

The equilibrium position of the aircraft at constant speed taxiing is taken as the coordinate origin. According to the ideal connection relationship among the three elements (inerter-spring-damper) studied in reference [17], combined with the structure of the landing gear buffer, and the taxiing dynamic model of single strut landing gear is established, as shown in Fig. 2. Where, m_s is the sprung mass, including the fuselage, wing, buffer outer cylinder and other parts; m_u is the unsprung mass, including the buffer piston rod, brake device, wheels, and other parts; k_1 and c_1 are the spring stiffness coefficient and damping coefficient of SDLG buffer, respectively; k_2 and c_2 are the spring stiffness coefficient and damping coefficient of the ISDLG buffer, respectively; k_3 is the stiffness coefficient of the deputy spring; k_t and c_t are the spring stiffness coefficient and damping coefficient of the tire, respectively; z_s and z_u are the vertical displacements of the sprung mass and the unsprung mass, respectively; z_r is the change of the road in the vertical direction.

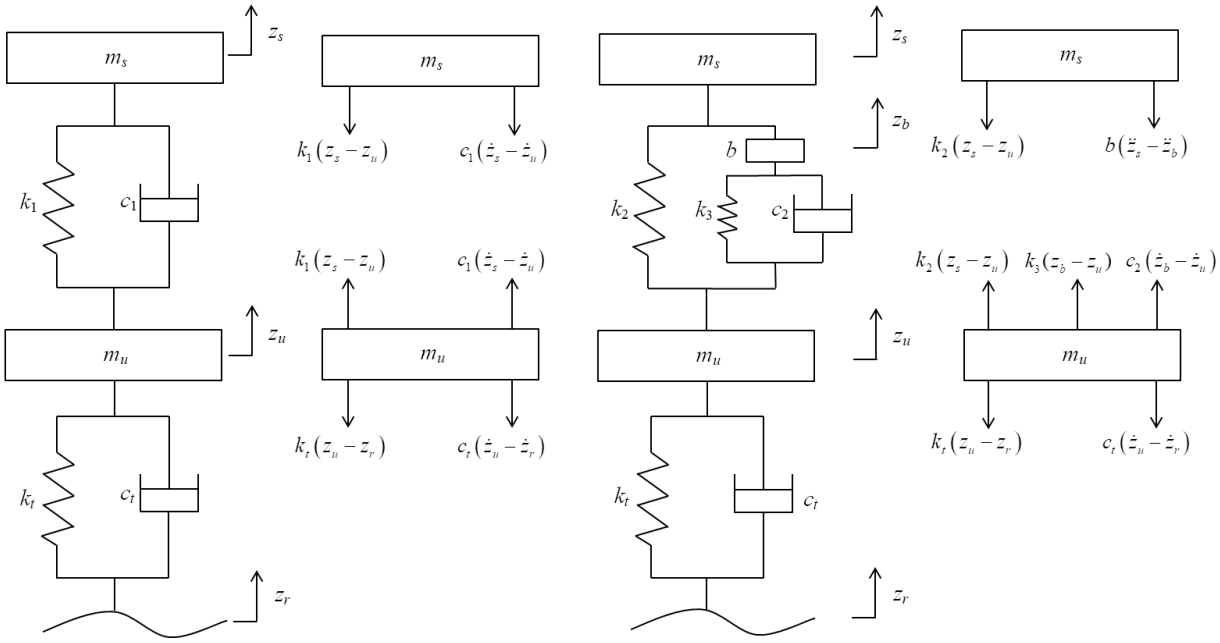

Fig. 2 Taxiing dynamic model of single strut landing gear: a) SDLG; b) ISDLG

When the aircraft is taxiing at a constant speed on the ground, in the vertical direction, the sprung mass and the unsprung mass are balanced under the combined action of lift, gravity, and the axial force of the buffer, respectively. When excited by the road surface, the two masses vibrate up and down respectively at their equilibrium positions. Therefore, the effects of lift and gravity cannot be considered when the aircraft starts at a constant speed taxiing state [15, 18]. According to Newton's second law, the differential equation of motion of the aircraft at the equilibrium position can be obtained as:

$$\begin{cases} m_s\ddot{z}_s + F_s = 0 \\ m_u\ddot{z}_u - F_s + F_t = 0 \end{cases}, \tag{2}$$

where: F_s is the buffering force, for the two models in Fig. 2, the sizes are:

$$F_{s1} = k_1\left(z_s - z_u\right) + c_1\left(\dot{z}_s - \dot{z}_u\right), \tag{3}$$

$$F_{s2} = k_2\left(z_s - z_u\right) + b\left(\ddot{z}_s - \ddot{z}_b\right) = k_2\left(z_s - z_u\right) + k_3\left(z_b - z_u\right) + c_2\left(\dot{z}_b - \dot{z}_u\right). \tag{4}$$

F_t is the dynamic tire load, and its size is:

$$F_t = k_t\left(z_u - z_r\right) + c_t\left(\dot{z}_u - \dot{z}_r\right). \tag{5}$$

The time domain model of road roughness shown in formula (6) is used as road surface excitation [18]:

$$\dot{z}_r(t) = -2\pi f z_r(t) + 2\pi n_0\sqrt{G_q(n_0)v}\,\omega(t), \tag{6}$$

where: f is the lower cut-off frequency in Hz; n_0 is the reference spatial frequency in m^{-1}; v is the taxiing speed in m/s; $\omega(t)$ is the Gaussian white noise; $G_q(n_0)$ is the road roughness coefficient in m^3. According to the power spectral density (PSD) of road surface, the road roughness is classified into eight grades A~H [19], and according to the international roughness index (*IRI*), the road roughness is evaluated in segments [20]. The relationship between *IRI* and $G_q(n_0)$ can be determined according to the following formula [21]:

$$IRI = 0.78\sqrt{G_q(n_0)}. \tag{7}$$

The state-space equation of model *a* is established as:

$$\begin{cases} \dot{X}_1 = A_1 X_1 + B_1 U_1 \\ Y_1 = C_1 X_1 + D_1 U_1 \end{cases}, \tag{8}$$

where: $X_1 = \begin{bmatrix} \dot{z}_s & \dot{z}_u & z_s & z_u \end{bmatrix}^T$; $U_1 = \begin{bmatrix} \dot{z}_r & z_r \end{bmatrix}^T$;

$Y_1 = \begin{bmatrix} \ddot{z}_s & z_s - z_u & k_t(z_u - z_r) + c_t(\dot{z}_u - \dot{z}_r) \end{bmatrix}^T$;

$$A_1 = \begin{bmatrix} -\frac{c_1}{m_s} & \frac{c_1}{m_s} & -\frac{k_1}{m_s} & \frac{k_1}{m_s} \\ \frac{c_1}{m_u} & -\frac{c_1 + c_t}{m_u} & \frac{k_1}{m_u} & -\frac{k_1 + k_t}{m_u} \\ 1 & 0 & 0 & 0 \\ 0 & 1 & 0 & 0 \end{bmatrix}; \quad B_1 = \begin{bmatrix} 0 & 0 \\ \frac{c_t}{m_u} & \frac{k_t}{m_u} \\ 0 & 0 \\ 0 & 0 \end{bmatrix};$$

$$C_1 = \begin{bmatrix} -\frac{c_1}{m_s} & \frac{c_1}{m_s} & -\frac{k_1}{m_s} & \frac{k_1}{m_s} \\ 0 & 0 & 1 & -1 \\ 0 & c_t & 0 & k_t \end{bmatrix}; \quad D_1 = \begin{bmatrix} 0 & 0 \\ 0 & 0 \\ -c_t & -k_t \end{bmatrix}.$$

The state-space equation of model *b* is established as:

$$\begin{cases} \dot{X}_2 = A_2 X_2 + B_2 U_2 \\ Y_2 = C_2 X_2 + D_2 U_2 \end{cases}, \tag{9}$$

where: $X_2 = \begin{bmatrix} \dot{z}_s & \dot{z}_u & \dot{z}_b & z_s & z_u & z_b \end{bmatrix}^T$;

$U_2 = \begin{bmatrix} \dot{z}_r & z_r \end{bmatrix}^T$;

$Y_2 = \begin{bmatrix} \ddot{z}_s & z_s - z_u & k_t(z_u - z_r) + c_t(\dot{z}_u - \dot{z}_r) \end{bmatrix}^T$;

$$A_2 = \begin{bmatrix} 0 & \frac{c_2}{m_s} & -\frac{c_2}{m_s} & -\frac{k_2}{m_s} & \frac{k_2 + k_3}{m_s} & -\frac{k_3}{m_s} \\ 0 & -\frac{c_2 + c_t}{m_u} & \frac{c_2}{m_u} & \frac{k_2}{m_u} & -\frac{k_2 + k_3 + k_t}{m_u} & \frac{k_3}{m_u} \\ 0 & \frac{c_2}{m_s} + \frac{c_2}{b} & -\left(\frac{c_2}{m_s} + \frac{c_2}{b}\right) & -\frac{k_2}{m_s} & \frac{k_2 + k_3}{m_s} + \frac{k_3}{b} & -\left(\frac{k_3}{m_s} + \frac{k_3}{b}\right) \\ 1 & 0 & 0 & 0 & 0 & 0 \\ 0 & 1 & 0 & 0 & 0 & 0 \\ 0 & 0 & 1 & 0 & 0 & 0 \end{bmatrix}; \quad B_2 = \begin{bmatrix} 0 & 0 \\ \frac{c_t}{m_u} & \frac{k_t}{m_u} \\ 0 & 0 \\ 0 & 0 \\ 0 & 0 \\ 0 & 0 \end{bmatrix};$$

$$C_2 = \begin{bmatrix} 0 & \frac{c_2}{m_s} & -\frac{c_2}{m_s} & -\frac{k_2}{m_s} & \frac{k_2 + k_3}{m_s} & -\frac{k_3}{m_s} \\ 0 & 0 & 0 & 1 & -1 & 0 \\ 0 & c_t & 0 & 0 & k_t & 0 \end{bmatrix}; \quad D_2 = \begin{bmatrix} 0 & 0 \\ 0 & 0 \\ -c_t & -k_t \end{bmatrix}.$$

3. ISDLG parameter optimization

For SDLG, the public data of aircraft landing gear is selected for simulation. For ISDLG, due to the introduction of *b* and k_3, it is necessary to optimize each parameter and then perform a simulation. Since the gas spring of the landing gear buffer needs to carry the fuselage's weight, k_2 is kept constant, and only three parameters, k_3, c_2, and *b* are optimized.

In order to reflect the buffering performance when the aircraft is taxiing on the ground, fuselage acceleration, buffer stroke, and dynamic tire load are selected as the performance indexes. Precisely, the fuselage acceleration reflects the ride comfort of the aircraft taxiing on the ground, the buffer stroke reflects whether the buffer is in the normal working stroke, and the dynamic tire load reflects the handling stability of the aircraft. However, since the above performance indexes do not exist independently and usually influence each other, it is not easy to obtain a solution to make each performance index optimal. Therefore, it is necessary to compromise each performance index to obtain the optimal global solution.

The genetic optimization algorithm is based on the natural selection principle, natural genetic mechanism, and adaptive search and optimization. Because of its strong robustness and global search ability, and its application and theoretical research in engineering tend to mature, this paper selects genetic optimization algorithm to solve the multi-parameter multi-objective optimization problem of ISDLG.

Firstly, the RMS values of ISDLG's fuselage acceleration, buffer stroke, and dynamic tire load are divided by the RMS values of SDLG's corresponding performance indexes to solve the problem that each single objective function units and orders of magnitude are not uniform. Then the linear weighting sum method was used to change the degree of emphasis on every single objective. Since the research object of this paper is passenger aircraft, more attention should be paid to the fuselage acceleration to improve the ride comfort for passengers. Then the buffer stroke and dynamic tire load should be considered. Therefore, the weight coefficients of the RMS values of performance indexes are 0.54, 0.13, and 0.33, respectively. Finally, the multi-objective optimization is transformed into a single-objective optimization:

$$minL = \frac{0.54BA_{ISD}}{BA_{SD}} + \frac{0.13SWS_{ISD}}{SWS_{SD}} + \frac{0.33DTL_{ISD}}{DTL_{SD}}. \tag{10}$$

In the formula, L is the fitness function; BA_{ISD}, SWS_{ISD}, and DTL_{ISD} are the RMS values of fuselage acceleration, buffer stroke, and dynamic tire load of ISDLG, respectively; BA_{SD}, SWS_{SD}, and DTL_{SD} are the RMS values of the corresponding performance indexes of SDLG.

The design variables are:

$$X = (k_3, c_2, b), \tag{11}$$

where, the interval values of design variables are:

$$\begin{cases} 0.1 < k_3 < 6.73\times10^5 \\ 0.1 < c_2 < 6.25\times10^4 \\ 30 < b < 5000 \end{cases}. \tag{12}$$

The constraints are:

$$\begin{cases} BA_{ISD} \le BA_{SD} \\ SWS_{ISD} \le SWS_{SD} \\ DTL_{ISD} \le DTL_{SD} \end{cases}. \tag{13}$$

The script of the genetic optimization algorithm is written in the MATLAB workspace. The population size is 50, the number of terminated evolutionary iterations is 20, the crossover probability is 0.8, and the mutation probability is 0.01. The simulation model is built in Simulink, as shown in Fig. 3. After many solutions and comparisons, the optimal values of the parameters to be optimized are obtained, as shown in Fig. 4. After rounding, the parameters are $k_3 = 2.1341\times10^5$, $b = 3910$ and $c_2 = 6.0119\times10^4$, and the remaining simulation parameters are shown in Table 1.

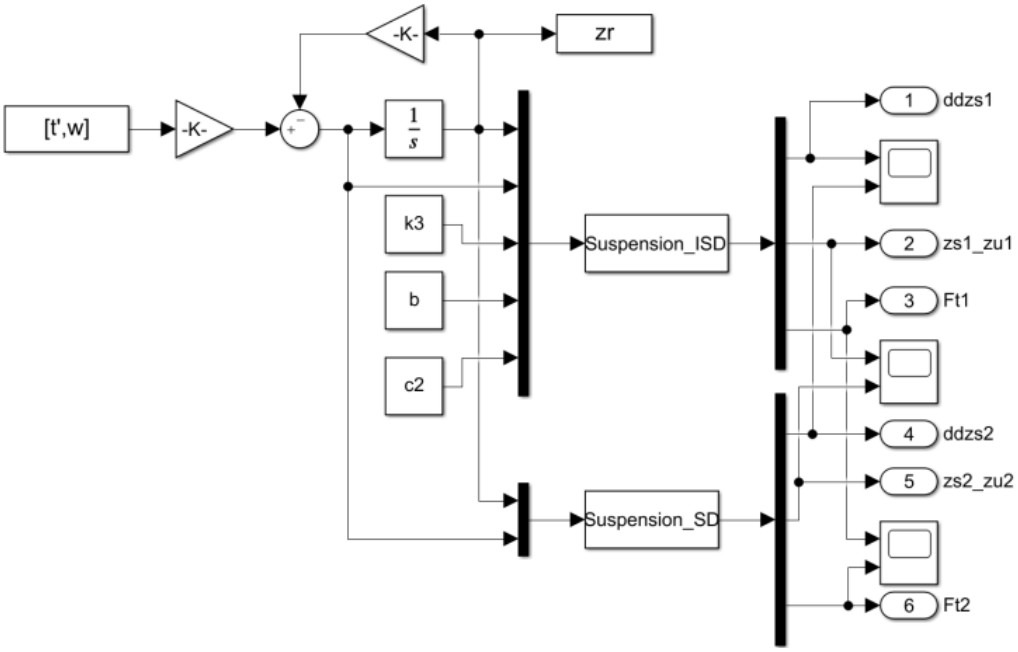

Fig. 3 Simulink implementation of single strut landing gear

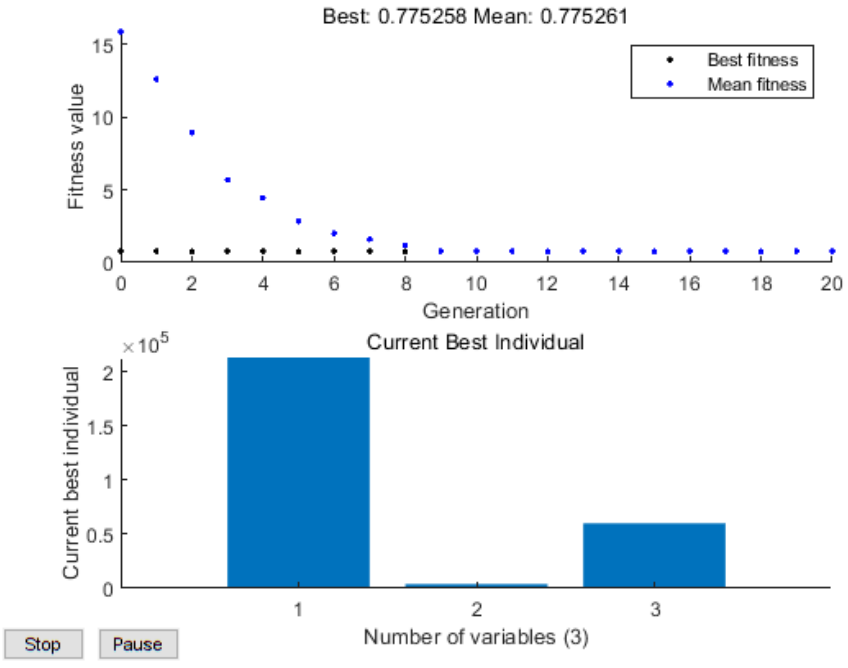

Fig. 4 Parameter optimization results

Table 1

Model parameters

Parameter	Symbol	Value	Unit
Sprung mass	m_s	2500	kg
Unsprung mass	m_u	260	kg
Spring stiffness coefficient of the tire	k_t	6.75×10^5	N/m
Damping coefficient of the tire	c_t	4066	N·s/m
Spring stiffness coefficient of SDLG buffer	k_1	6.73×10^5	N/m
Damping coefficient of SDLG buffer	c_1	1.63×10^4	N·s/m
Spring stiffness coefficient of ISDLG buffer	k_2	6.73×10^5	N/m
Lower cut-off frequency	f	0.01	Hz
Reference space frequency	n_0	0.1	m^{-1}
Coefficient of road roughness	$G_q(n_0)$	256×10^{-6}	m^3

4. Simulation analysis

4.1. Time domain analysis

The aircraft is assumed to taxi for 10 s at a constant speed of 30 m/s on the C-grade road surface (*IRI*=12.48), and the sampling interval is 0.005 s. Fig. 5 depicts the random road surface excitation, while Fig. 6 and Tables 2 and 3 display the time domain output results of performance indexes.

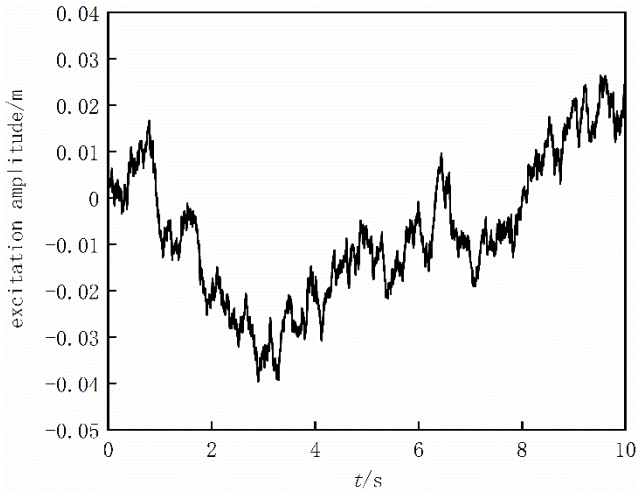

Fig. 5 Random road surface excitation

As seen from Fig. 6 and Table 2, the peak values of the performance indexes of ISDLG are smaller than those of SDLG.

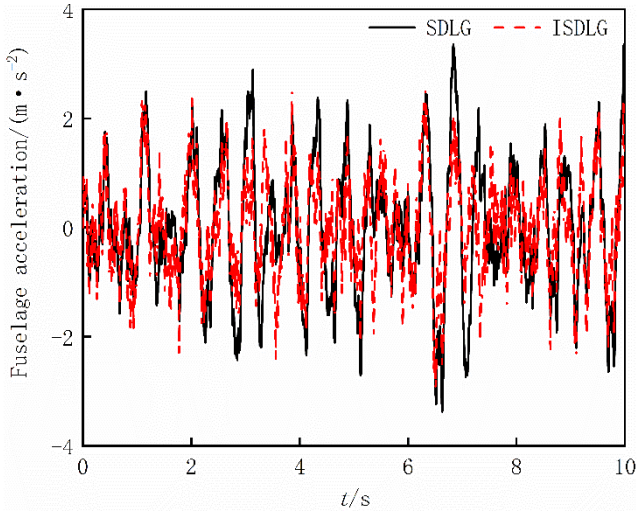

a

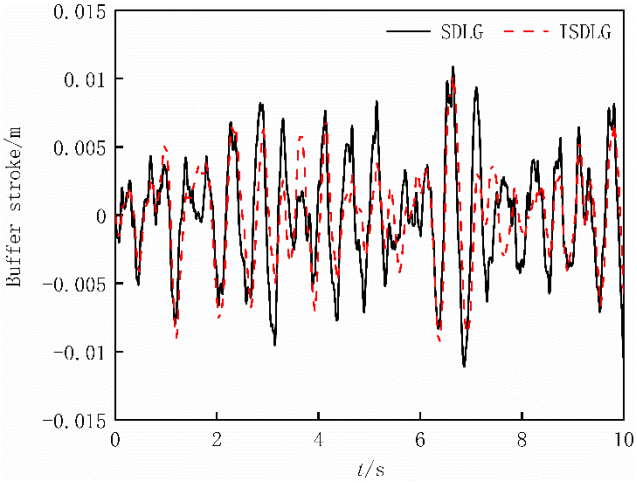

b

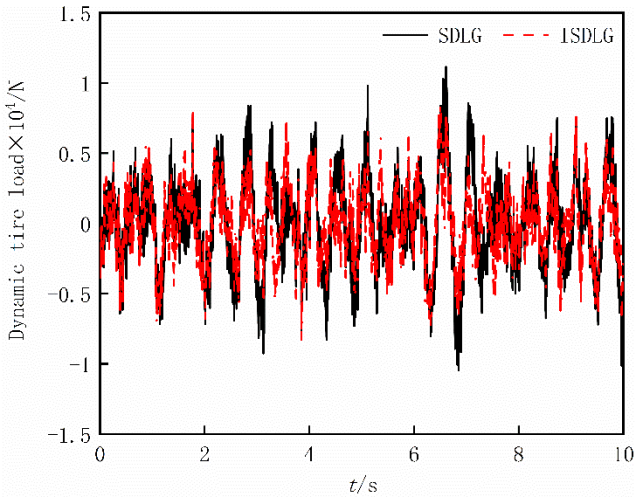

c

Fig. 6 Comparison of performance indexes: a) fuselage acceleration; b) buffer stroke; c) dynamic tire load

Specifically, the peak value of fuselage acceleration is reduced by about 12.60%, the peak value of buffer stroke is not changed much, reduced by about 8.11%, and the peak value of dynamic tire load is reduced by about 24.48%. It can be seen from Table 3 that compared with SDLG, the RMS value of the fuselage acceleration of ISDLG is reduced by about 24.96%, the RMS value of the buffer stroke is reduced by about 12.20%, and the RMS value of the dynamic tire load is reduced by about 21.87%, which effectively improves the ride comfort and handling stability of the aircraft during taxiing.

Table 2

Peak values of performance indexes

Buffer structure	Fuselage acceleration, m·s^{-2}	Buffer stroke, m	Dynamic tire load, N
SDLG	3.3746	0.0111	11150
ISDLG	2.9459	0.0102	8420
Decreasing amplitude,%	12.60	8.11	24.48

Table 3

RMS values of performance indexes

Buffer structure	Fuselage acceleration, m·s^{-2}	Buffer stroke, m	Dynamic tire load, N
SDLG	1.2146	0.0041	3305.2
ISDLG	0.9114	0.0036	2582.4
Decreasing amplitude,%	24.96	12.20	21.87

4.2. Frequency domain analysis

The two models are simulated in the frequency domain, and the sampling frequency is 1000 HZ. The PSD of each performance index in the range of 0~15 HZ is obtained, as shown in Fig. 7.

It can be seen from Fig. 7 that compared with SDLG, the peak values of PSD of ISDLG's fuselage acceleration, buffer stroke, and dynamic tire load in the low frequency range of 0~3 HZ are all decreased significantly, while there is no significant change in the high frequency range.

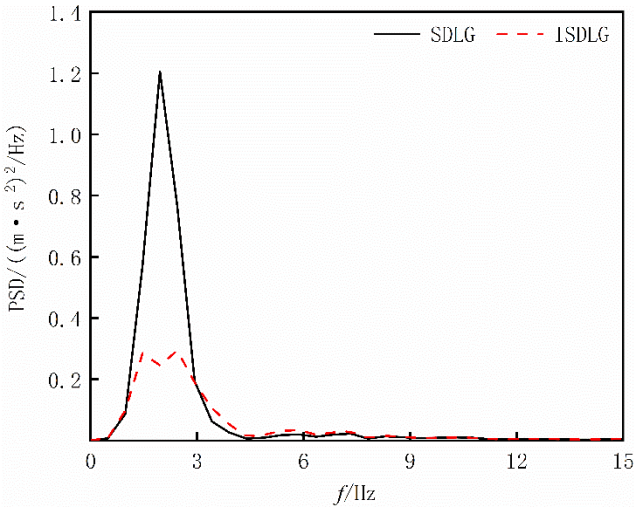

a

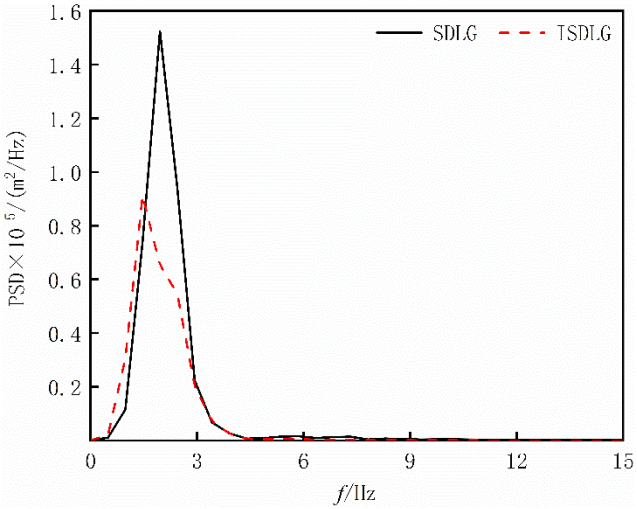

b

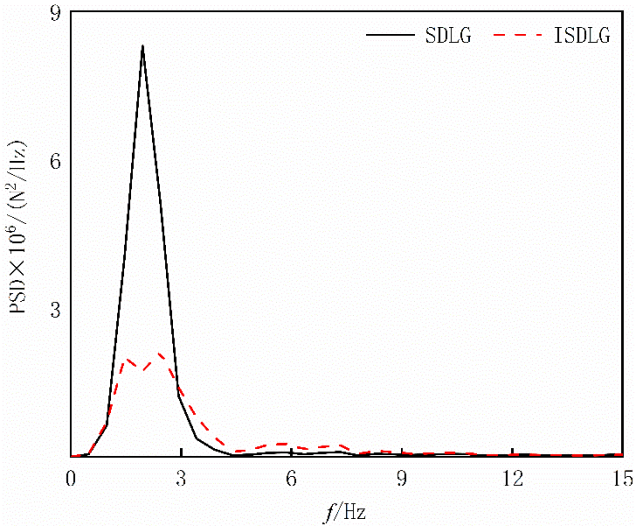

c

Fig. 7 Comparison of PSD of performance indexes: a) PSD of fuselage acceleration; b) PSD of buffer stroke; c) PSD of dynamic tire load

This indicates that ISDLG can effectively suppress the low frequency vibration of the fuselage, and reflects that the inerter has the characteristics of passing the high frequency and blocking the low frequency.

4.3. Analysis of the influence of different speeds and road grades on performance

When the aircraft is taxiing on the airport runway, forced vibration of the fuselage caused by uneven road surface excitation is related to not only the aircraft's structural parameters but also the speed and the road grade.

In this paper, *IRI*=2~5 is selected to represent four different road grades, as shown in Table 4. In order to reflect the situation of the aircraft taxiing at low and high speeds, the simulation speed range of 0~70 m/s is selected with 10 m/s as the interval. Fig. 8 depicts the variation trend of performance indexes of the two models at different speeds on different road grades.

It can be seen from Fig. 8 that when the speed is constant, the worse the road grade is, the bigger the RMS values of performance indexes of the two models are; when the road grade is fixed, the faster the speed is, the bigger the RMS values of the performance indexes of the two models are. The RMS values of performance indexes of ISDLG are smaller than those of SDLG at the same speed and road grade. Specifically, the RMS values of

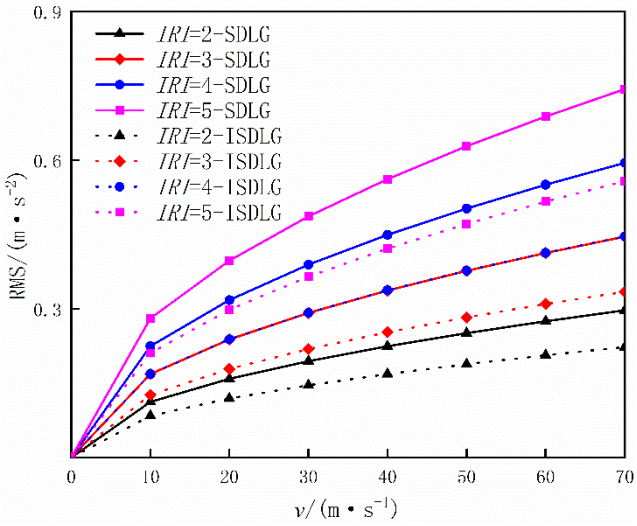

a

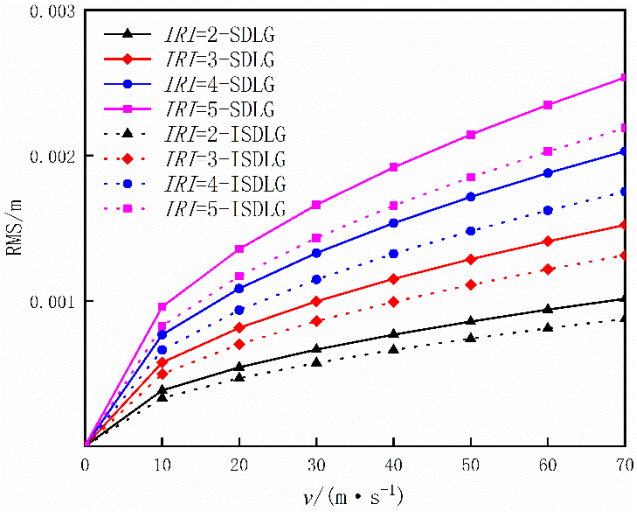

b

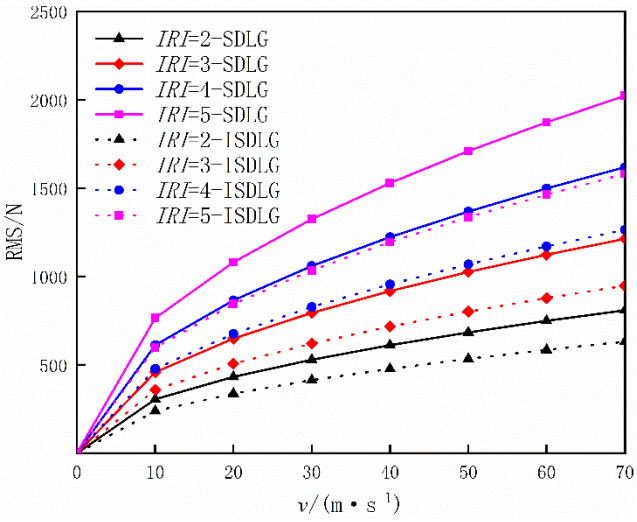

c

Fig. 8 The influence of different speeds and road grades on performance indexes: a) RMS values of fuselage acceleration; b) RMS values of buffer stroke; c) RMS values of dynamic tire load

fuselage acceleration, buffer stroke, and dynamic tire load are reduced by a maximum of 24.96%, 14.08%, and 21.87%, respectively. In addition, when the speed is constant, the RMS values of performance indexes of ISDLG under poor road grades are close to or even smaller than those of SDLG under good road grades. For example, the RMS values of fuselage acceleration and dynamic tire load of ISDLG with *IRI*=4 are close to or even basically the same as those of SDLG with *IRI*=3. The RMS values of fuselage acceleration and dynamic tire load of ISDLG with *IRI*=5 are close to those of SDLG with *IRI*=4. This demonstrates that ISDLG can effectively improve the vibration caused by the deterioration of the road grade.

Table 4

IRI and $G_q(n_0)$ at different road grades

Excellent (*IRI*<2.5)		Good (2.5<*IRI*<3.5)		Average (3.5<*IRI*<4.3)		Poor (*IRI*>4.3)	
IRI	$G_q(n_0)$	*IRI*	$G_q(n_0)$	*IRI*	$G_q(n_0)$	*IRI*	$G_q(n_0)$
2.00	6.57	3.00	14.79	4.00	26.30	5.00	41.09

5. Conclusions

1. The taxiing dynamic models of SDLG and ISDLG are established, respectively, and the structural parameters of ISDLG are optimized using a multi-objective genetic optimization algorithm.

2. The two models are simulated and analyzed from the time domain and frequency domain. The results show that the peak values and RMS values of fuselage acceleration, buffer stroke, and dynamic tire load of ISDLG are all lower than those of SDLG, especially at low frequencies. This demonstrates that ISDLG can effectively suppress the low frequency vibration of the fuselage and improve the ride comfort and handling stability of the aircraft when it taxis on the ground.

3. The influence laws of different speeds and road grades on performance indexes are analyzed. The results show that the performance indexes of the two models will deteriorate with the increase of speed and the deterioration of road grade, but the extent to which performance indexes of ISDLG are superior to those of SDLG is increasingly evident. In addition, through comparison, it is found that ISDLG can effectively improve the vibration caused by the deterioration of the road grade.

References

1. **Wei, X.** 2005. Dynamic analysis of aircraft landing impact and vibration attenuating techniques, Nanjing University of Aeronautics and Astronautics, China. https://doi.org/10.7666/d.d016042.
2. **Li, X.** 2004. Integration of shock performance analysis, design of aircraft landing gears, Northwestern Polytechinical University, China. https://doi.org/10.7666/d.y585255.
3. Aircraft design manual, Aircraft Design Manual Compilatory Committee, 2002.
4. **Smith, M. C.** 2002. Synthesis of mechanical networks: the inerter, IEEE Transactions on Automatic Control 47(10): 1648-1662.

https://doi.org/10.1109/TAC.2002.803532.
5. **Smith, M. C.; Wang, F.** 2004. Performance benefits in passive vehicle suspensions employing inerters, Vehicle System Dynamics 42(4): 235-257. https://doi.org/10.1080/00423110412331289871.
6. **Wang, F.; Liao, M.; Liao, B.;** et al. 2009. The performance improvements of train suspension systems with mechanical networks employing inerters, Vehicle System Dynamics 47(7): 805-830. https://doi.org/10.1080/00423110802385951.
7. **Wang, F.; Hong, M.; Chen, C.** 2010. Building suspensions with inerters, Proceedings of the Institution of Mechanical Engineers, Part C: Journal of Mechanical Engineering Science 224(8): 1605-1616. https://doi.org/10.1243/09544062JMES1909.
8. **Dong, X.; Liu, Y.; Chen, M.** 2015. Application of inerter to aircraft landing gear suspension, IEEE 34th Chinese Control Conference, p. 2066-2071. https://doi.org/10.1109/ChiCC.2015.7259953.
9. **Liu, Y.; Chen, M.; Tian, Y.** 2015. Nonlinearities in landing gear model incorporating inerter, IEEE International Conference on Information and Automation, p. 696-701. https://doi.org/10.1109/ICInfA.2015.7279375.
10. **Li, Y.; Jiang, J.; Neild, S.** 2017. Inerter-based configurations for main-landing-gear shimmy suppression, Journal of Aircraft 54(2): 684-692. https://doi.org/10.2514/1.C033964.
11. **Li, Y.; Howcroft, C.; Neild, S.;** et al. 2017. Using continuation analysis to identify shimmy-suppression devices for an aircraft main landing gear, Journal of Sound and Vibration 408: 234-251. https://doi.org/10.1016/j.jsv.2017.07.028.
12. **Li, Y.; Jiang, J.; Neild, S.;** et al. 2017. Optimal inerter-based shock-strut configurations for landing-gear touchdown performance, Journal of Aircraft 54(5): 1901-1909. https://doi.org/10.2514/1.C034276.
13. **Xu, F.; Kong, W.; Song, C.** 2018. Analysis of aircraft taxiing dynamics with different pavement roughness, Computer Simulation 35(10): 104-108.
14. **Qian, J.; Pan, X.; Cen, Y.;** et al. 2022. Aircraft taxiing dynamic load induced by runway roughness, Journal of Vibration and Shock 41(20): 176-184+269. https://doi.org/10.13465/j.cnki.jvs.2022.20.022.
15. **Zhang, Y.** 2018. Research on ISD-based landing gear taxiing dynamics and fatigue damage detection of key components, National University of Defense Technology, China. https://doi.org/10.27052/d.cnki.gzjgu.2018.001249.
16. **Smith, M. C.** 2020. The inerter: a retrospective, Annual Review of Control Robotics and Autonomous Systems 3(1): 361-391. https://doi.org/10.1146/annurev-control-053018-023917.
17. **Chen, L.; Yang, X.; Wang, R.;** et al. 2013. Design and performance study of vehicle passive suspension based on two-element inerter-spring-damper structure vibration isolation mechanism, Journal of Vibration and Shock 32(06): 90-95. https://doi.org/10.13465/j.cnki.jvs.2013.06.028.
18. **Lei, J.; Shi, X.; Cai, L.;** et al. 2020. A quarter landing gear taxiing model based on filtered white noise method, Journal of Air Force Engineering University (Natural Science) 21(03): 12-18. https://doi.org/10.3969/j.issn.1009-3516.2020.03.003.
19. Mechanical Vibration-Road Surface Profiles-Reporting of Measured Data. GB/T 7031-2005. National Technical Committee for Standardization of Mechanical Vibration and Shock, 2005.
20. Specifications for Pavement Evaluation and Management of Civil Airports. MH/T 5024-2019. Civil Aviation Administration of China, 2019.
21. **Huang, L.; Sheng, C.** 2006. Relationship between vehicle dynamic amplification factor and pavement roughness, Journal of Highway and Transportation Research and Development (03): 27-30. https://doi.org/10.3969/j.issn.1002-0268.2006.03.007.

Y. Wang, C. Zhang, P. Wang, X. Cao, Z. Ge

ANALYSIS OF TAXIING PERFORMANCE OF SINGLE STRUT LANDING GEAR BASED ON ISD

S u m m a r y

In this paper, the inerter is introduced to form the "inerter-spring-damper" landing gear (ISDLG) based on the "spring-damper" landing gear (SDLG), and the taxiing dynamic models of both are established. Taking fuselage acceleration, buffer stroke, and dynamic tire load as performance indexes, the parameters of the ISDLG are optimized using a multi-objective genetic optimization algorithm. In MATLAB/Simulink environment, SDLG and ISDLG are simulated in the time domain and frequency domain. The results show that compared with SDLG, the values of performance indexes of ISDLG are all reduced, especially at low frequencies. This demonstrates that ISDLG can effectively suppress the low frequency vibration of the fuselage and improve the ride comfort and handling stability of the aircraft when it taxis on the ground. In addition, the performance indexes of the two models will deteriorate with the increase of speed and the deterioration of road grade, but the extent to which performance indexes of ISDLG are superior to those of SDLG is increasingly evident. Through comparison, it is also found that ISDLG can effectively improve the vibration caused by the deterioration of the road grade.

Keywords: inerter, ISDLG, taxiing, parameter optimization, simulation.

Received March 6, 2023
Accepted December 3, 2023